Research Article

Journal of Environmental Nanotechnolog

Photocatalytic Activity of PVA Modified TiO_2 Nanoparticles

K. Balachandran[1*], R. Mariappan[2], S. Vijayan[3]

[1]Department of Chemistry, Vivekanandha College of Engineering for Women, Tiruchengode, TN, India.
[2]Department of Physics, Adhiyamaan College of Engineering, Hosur, TN, India.
[3]Department of Physics, M. G. R. Arts & Science College, Hosur, TN, India.
Received: 12.11.2017 Accepted: 15.01.2018
*balanano06@gmail.com

ABSTRACT

A novel, less time consuming and cost-ineffective Wet chemical technique (WCT) was used to synthesise polyvinyl alcohol (PVA) modified TiO_2 nanoparticles at relatively low temperature, in acidic pH, using Titanium tetra isopropoxide (TTIP) as a precursor. The synthesized nanoparticles were characterized by XRD, SEM-EDAX, TEM, FTIR and Uv-Visible spectroscopy. The results show that increasing PVA concentration reduces the particle size from 17 nm to 10 nm and increase the surface area from 54 to 65 m^2/g. The Uv-Visible spectra show that blue shift was observed in all nanoparticles, which indicates PVA have the capability to control the particle size. The TEM images revealed that all the particles were in nanometer size. The synthesized nanoparticles show good photocatalytic activity, and they decompose textile dye isolan blue (IB) in 5 hr reaction.

Keywords: Isolan blue; Photocatalytic activity; Surface area; Wet chemical technique.

1. INTRODUCTION

Due to the rapid increase in dyeing industries, water contamination increases day by day. To solve this problem, conventional treatments like adsorption on activated carbon, ultrafiltration, reverse osmosis, coagulation by chemical agents, and ion exchange process have been used for the dye pollutants (Konstantinou and Albanis, 2004; Tang and An, 1995; Selvaraj *et al*. 2013). These methods only succeed in transferring organic compounds from water to another phase. Thus it creates secondary pollution (Akpan and Hameed, 2009). Further, it will require another treatment for the removal of solid waste.

Due to these reasons, considerable attention has been focused on the complete oxidation of organic compounds to harmless products such as CO_2 and H_2O by advanced oxidation process (AOP) (Mahadwad *et al.* 2011), which include ozonolysis, sono catalysis, photocatalysis, photo Fenton and photo electro Fenton process have emerged as popular techniques to decompose the contaminants from wastewater (Sushil Kumar Kansal *et al.* 2013).

Heterogeneous photocatalysis has shown high efficiency in the removal of highly toxic and non-biodegradable pollutants commonly present in the air and in domestic or industrial wastewaters (Herrmann, 1999; Hoffmann *et al.* 1995). These processes are based on the use of UV radiation to stimulate a semiconductor material, usually, TiO_2, on whose surface oxidation of the pollutants is carried out.

Titanium dioxide (TiO_2), is one of the most popular and promising materials in photocatalytic application due to the strong oxidizing power of its holes, high photostability and redox selectivity (Fox and Dulay, 2004; Shankar *et al.* 2004), TiO_2 nanocrystalline is one of the most popular photocatalysts, has long been investigated for environmental purification studies (Fujishima *et al.* 2000; Beydoun *et al.* 1999). Recent studies show that the photocatalytic activity of TiO_2 depends strongly on its grain size (Zhang and Zheng, 2008). The decrease of grain size implies an increase in surface area and high redox potential, which leads to high photocatalytic activity. Therefore, much more attention has been focused on the preparation of nanocrystalline TiO_2 with unique properties of nanoparticles and their relations to photocatalytic properties. The Sol-gel technique has been widely used for the synthesis of nanophase TiO_2. Because of synthesis from atomic or molecular precursors, the sol-gel technique can give better control of particle size and homogeneity in particle distribution (Kumar *et al.* 1994; Bao *et al.* 2005; Music *et al.* 1997; Hsuan-Fu and Shenq-Min, 2000; Garbassi and Balducci, 2001; Gomez *et al.* 2003; Hussain *et al.* 2010; Nguyen and Vinh Nguyen, 2009; Vilma *et al.* 2004).

In the present work, we study the photocatalytic decomposition of isolan blue by PVA modified TiO_2 nanoparticles. The nanoparticles were synthesized by WCT and it was characterized by XRD, SEM-EDAX, TEM, FTIR and Uv-Visible spectroscopy.

2. EXPERIMENTAL METHODS

2.1 Materials

All reagents used were of analytical grade purity and were procured from Merck Chemical Reagent Co. Ltd. India.

2.2 Synthesis of TiO_2 and PVA modified TiO_2nanoparticles

A wet chemical (Sol-gel) technique was used to synthesis of TiO_2 nanoparticles. TTIP (Titanium tetra-isopropoxide) was used as a precursor, HCl as peptizing agent and C_2H_5OH was used as a solvent medium. 5 ml of HCl was mixed with 50 ml ethanol, and it was stirred for few minutes. To this mixture, 50 ml TTIP was added, and it was stirred for 1 hour at room temperature. Then 100 ml of distilled water was added, the temperature was raised to 50^{o}C and stirring was continued for 3 hours until the solution changed into a colourless gel. The high viscous gel was dried at room temperature to a fine powder. The resulting powder was heated at 120 ^{o}C for 1 hour in a hot air oven to remove the moisture and solvents. Finally, the colourless powder was calcined at 400 ^{o}C for 1 hour to increase the crystallinity and to remove the carbonaceous materials present in TTIP.

TiO_2 sol was prepared by the above-said method. PVA (molecular weight 2000) solutions were prepared by using de-ionised water. After the formation of TiO_2 sol, 10 ml of the prepared PVA solutions at different concentrations (1, 2 and 3%) were added under vigorous stirring to get a homogeneous solution. (By increasing the PVA concentration about 4 and 5%, the solutions form a precipitate, gets agglomerated, and it was difficult to stir the solution. So we fix the PVA concentration only upto 3%). The mixture was stirred for 3 hr and dried at room temperature. The colourless PVA modified TiO_2 nanoparticles were dried in a hot air oven at 120 ^{o}C for 1 hr. Finally, all the PVA modified TiO_2 nanoparticles were calcined at 400 ^{o}C to remove the PVA and increase the crystallinity.

2.3 Characterization

The prepared nanoparticles were characterized for the crystalline structure using D8 Advance X-ray diffraction meter (Bruker AXS, Germany) at room temperature, operating at 30 kV and 30 mA, using Cu$K\alpha$ radiation (λ = 0.15406 nm). The crystal size was calculated by Scherrer's formula. Surface morphology was studied by using SEM-EDS (Model JSM 6390LV, JOEL, USA), UV–Vis diffuse reflectance spectra were recorded with a Carry 5000 UV-Vis-NIR spectrophotometer (Varian, USA) and FTIR spectra were measured on an AVATAR 370-IR spectrometer (Thermo Nicolet, USA) with a wavenumber range of 4000 to 400 cm^{-1}. The surface area, pore size and pore volume of the nanocomposites was analyzed using BET analyser model Micromeritics Gemini 2375, Surface Area Analyser (Micromeritics Inc., Norcross, GA).

2.4 Measurement of Photocatalytic activity

The photocatalytic activity of the as-prepared particles for the environmental application was evaluated by measuring the photodegradation of isolan blue (IB) in water under sunlight irradiation. The initial concentration of IB was 50 mgl^{-1} and the concentration of TiO_2 was 25 mg l^{-1}.

3. RESULTS AND DISCUSSION

3.1 Phase and Grain size analysis

The effect of the polymer composition on the crystallite size and phase analysis was investigated by performing XRD analysis. Initially, all the samples exhibited an amorphous phase. Calcination was a common treatment to improve crystallinity. After calcination at 400 °C, the intensity of the peak increased and the phase transformed from amorphous to polycrystalline anatase (Hsuan-Fu and Shenq-Min, 2000). The increase of calcination temperature forced condensation of free -OH groups on the surface of TiO_2 particles. It increased the crystallinity and also the intensity of diffraction peaks of the anatase phase. The pH was also an important factor, which plays a role in nanoparticle synthesis. All the composites were synthesized at pH 2.

The XRD patterns of TiO_2 and PVA (1, 2 and 3%) modified TiO_2 particles before and after calcination are shown in Fig.1a and 1b, respectively. In the entire spectrum, sharp peak was obtained at 25.4°, which was a characteristic (101) reflection of the anatase phase. From Fig. 1b it can clearly be observed that increase in calcination temperature upto 400 °C, the peak intensity of anatase increases and the width of (101) plane, the diffraction peak of anatase (2θ=25.4°) became narrow (Yusuf *et al.* 2002; Hua *et al.* 2008). After calcination, the TiO_2 and PVA modified TiO_2 particles show Bragg's reflections at about 2θ = 25.4^o, 37.8^o, 48.3^o and 54.3^o peaks corresponding to (101), (004), (200) and (211) referred to as tetragonal crystal planes of anatase phase TiO_2 (Wang *et al.* 2006).

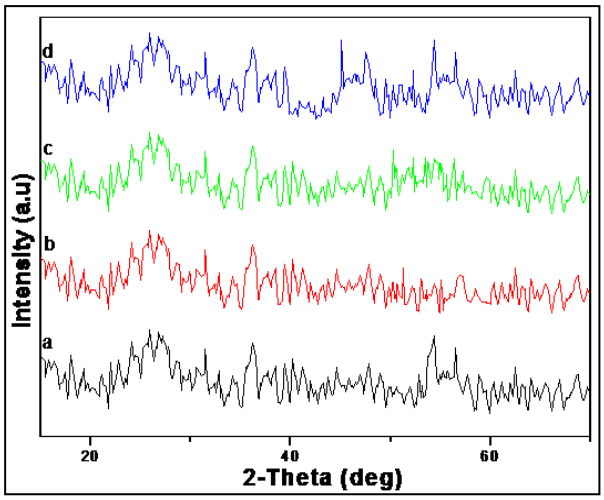

Fig. 1a: XRD patterns of a) TiO_2 b) 1% PVA c) 2% PVA and d) 3% PVA modified TiO_2 nanoparticles before calcinations

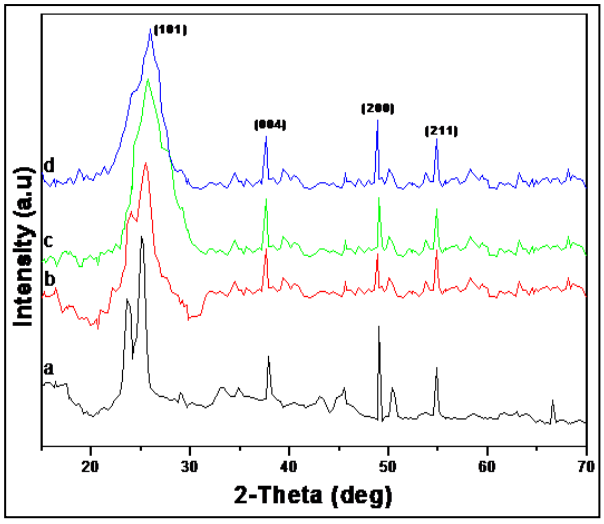

Fig. 1b: XRD patterns of a) TiO_2 b) 1% PVA c) 2% PVA and d) 3% PVA modified TiO_2 nanoparticles after calcination

The crystallite size of the as-prepared TiO_2 and PVA (1, 2 and 3%) modified TiO_2 was calculated for the (101) reflections by using Scherrer's equation.

$$D = \frac{k\lambda}{\beta \cos\theta} \qquad (1)$$

where k is the shape factor usually (k=0.94), λ is the X-ray wavelength, and β is the full width in radian at half maximum of the peak, and θ is the Bragg's angle of the X-ray diffraction peak.

The crystallite size of pure TiO_2 was 17 nm, and the crystallite size decreased with increasing concentration of PVA. The crystallite size of PVA modified TiO_2 particles were 14, 13 and 10 nm for 1, 2 and 3% PVA, respectively. The minimum crystallite size was obtained as 10 nm for 3% PVA modified TiO_2 particles. From the above discussions, it is clearly noted that the polymer i.e. PVA is a good medium to suppress the crystallite growth.

The lattice constants 'a' and 'ca were calculated by using the following expression.

$$\frac{1}{d^2} = \frac{(h^2 + k^2)}{a^2} + \frac{l^2}{c^2} \qquad (2)$$

The values of lattice constants 'a' of the TiO_2 nanoparticles are found to be (a=4.598 Å and c=2.950 Å) for 100 °C and (a=4.605 Å and c=2.945 Å) for 400 °C. It is found that the lattice constants 'a' and 'c' values are in good agreement with the standard values taken from JCPDS data card no. 89 4921. The dislocation density and microstrain were calculated using equations (3) and (4) for the TiO_2 nanoparticles.

$$\delta = \frac{1}{D^2} lines / m^2 \qquad (3)$$

$$\varepsilon = \frac{\lambda}{D \sin\theta} - \frac{\beta}{\tan\theta} \qquad (4)$$

It is observed that the dislocation density and microstrain for the (1 0 1) orientation plane decreases with the increase of PVA, and the same may be due to the release of stress in the nanoparticles.

3.2 Surface morphology analysis

A scanning electron microscope (SEM) was used to examine the surface morphology of the sol-gel prepared PVA modified TiO_2 particles. The SEM image of pure TiO_2 is shown in Fig. 2a. The pure TiO_2 nanoparticles exhibited an irregular morphology with non-uniform size distribution due to agglomeration of primary particles. The agglomeration of particles originated from the high surface energy and less number of surface states associated with the materials.

The nature of the interaction between anion and cation in the synthesized materials may also induce the agglomeration and non-uniform size distribution of particles.

The SEM images of PVA modified TiO_2 particles are shown in Fig. 2b, c and d. It is clearly observed that all the particles exhibited an irregular morphology and highly agglomerated white particles with non-uniform size distributions. However, with the increase in the PVA concentration, the composites showed a larger sized cluster of TiO_2 particles. It can be clearly observed that all the particles showed irregular morphology with non-uniform size distribution.

In order to obtain more detailed structural information, TEM analysis was performed. The TEM images of as-prepared PVA modified TiO_2 particles are

shown in Fig. 3. The TEM analysis of the PVA modified TiO_2 particles revealed a highly clustered nature. TEM analysis strongly supported the nanophase formation of TiO_2 particles. The average particle size measured from TEM was found to be in the range of 10-20 nm, which slightly varied from the particle size evaluated from XRD analysis. It was assumed that the crystallites were formed without any local strain. The selected area electron diffraction analysis (SAED) shows those continuous ring patterns which originate from polycrystalline state or by the more crystallites attached to the surface of the single particles. The bright ring pattern shows a high density of crystallites present in the composites.

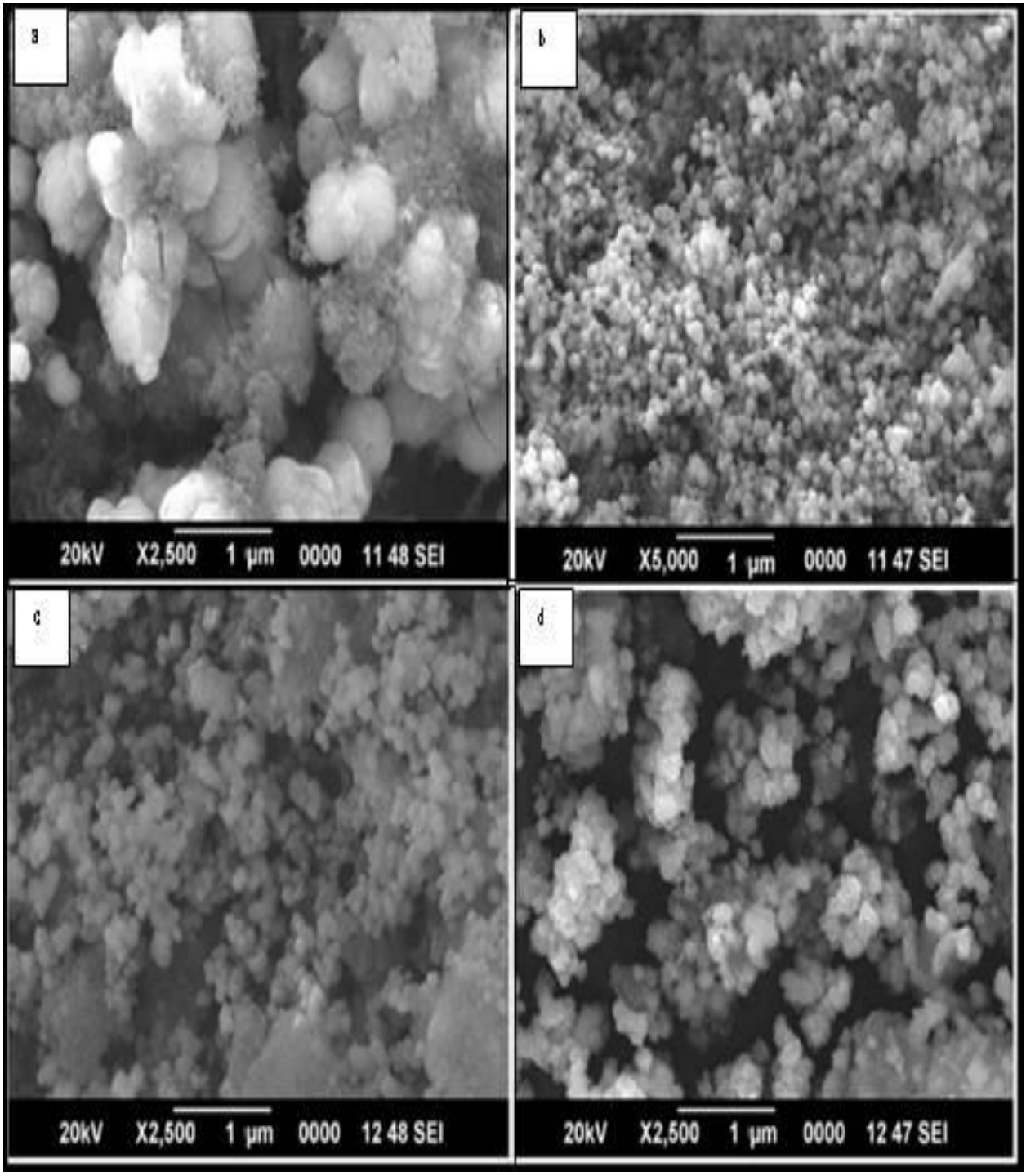

Fig. 2: SEM images of a) TiO_2 b) 1% PVA c) 2% PVA and d) 3% PVA modified TiO_2 nanoparticles

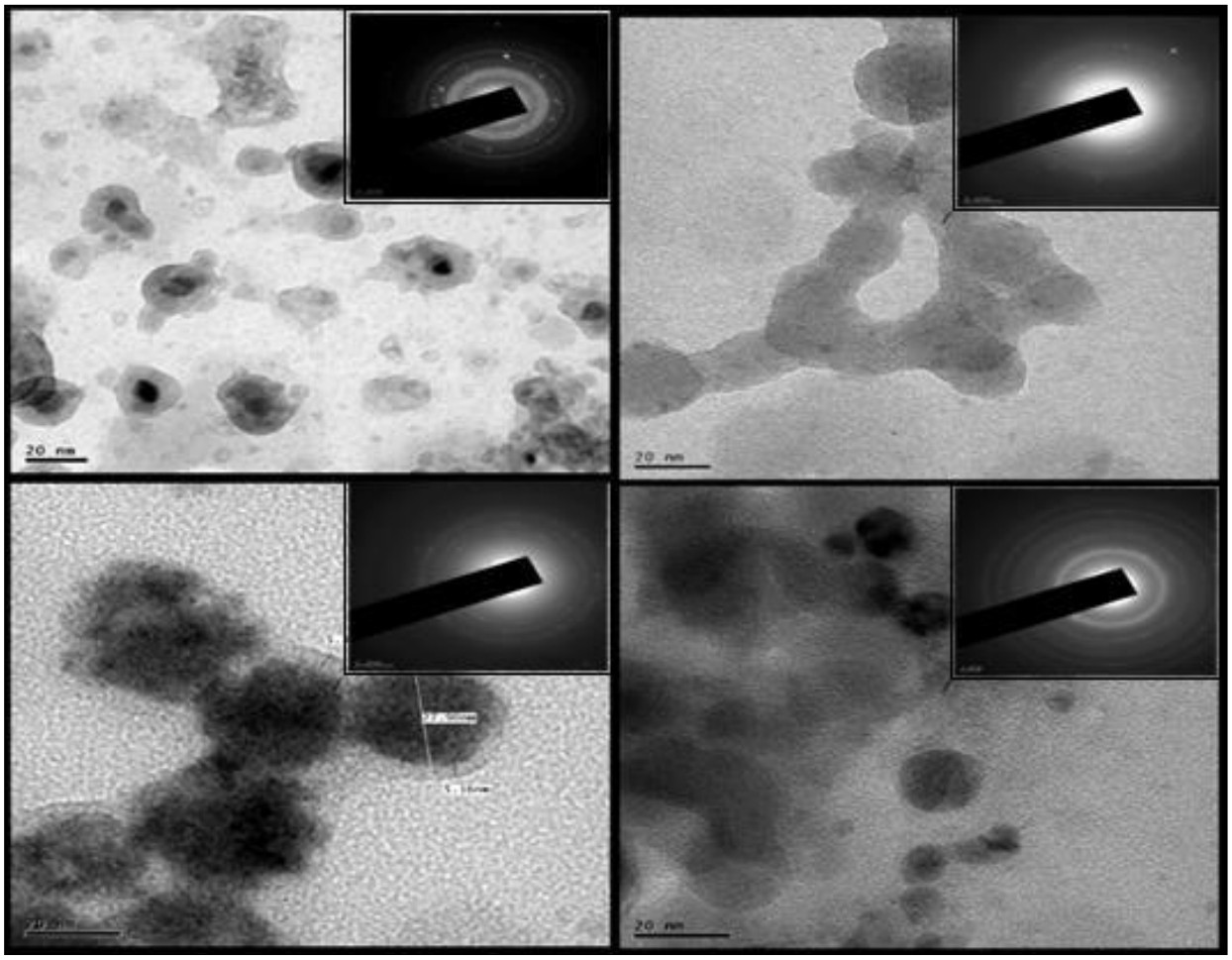

Fig. 3: TEM images of a) TiO_2 b) 1% PVA c) 2% PVA and d) 3% PVA modified TiO_2 nanoparticles

3.3 Elemental analysis

The EDAX spectra confirm the presence of Ti and O in TiO_2 and PVA modified TiO_2 nanoparticles, and it is shown in Fig.4. The energy versus counts graphs shows the presence of Ti and O atoms. In all samples, TiO_2 possessed a marginally high concentration of titanium cations than the oxygen anions, which is attributed to the intensity of peaks. In PVA modified TiO_2 nanoparticles, titanium and oxygen were present in the ratio of 4:1. This data strongly suggests that presence of Ti and O. Further, the presence of metal oxide bonds in all the composites were confirmed by FTIR spectra.

3.4 Fourier Transform Infra-Red Spectroscopy

The FT-IR spectrum of TiO_2 and PVA modified TiO_2 particles were recorded in the spectral range of 400-4000 cm^{-1}. Fig. 5 shows the FT-IR spectra of PVA modified TiO_2 particles. In all the spectrum, the bands observed at 3400 and 1600 cm^{-1} was assigned to the presence of -OH group of absorbed water and hydroxyl group on the surface of the catalyst. In all, the spectrum band observed around 1600 cm^{-1} was due to the bending vibrations of the -OH bond of chemisorbed water, and the band observed around 3400 cm^{-1} was due to the stretching mode of the -OH bond of free water. The absorption band observed in the entire spectrum at 1400 cm^{-1} is attributed to the Ti-O-Ti vibration. The wide absorption band observed in the spectral region of 500-900 cm^{-1} is related to Ti-O bonds inhomogeneous powder of TiO_2. In the entire spectrum, the broadband at 645-650 cm^{-1} corresponds to Ti-O-Ti stretching motion, and these strongly suggest the formation of TiO_2 particles (Dong *et al.* 2008). The band obtained at 1380 cm^{-1} indicate the presence of the semi-crystalline anatase phase for TiO_2, and the band observed at 512 cm^{-1} in all the spectrum corresponds to the characteristic anatase peaks (Malladi *et al.* 2006). In all samples, there are no characteristic peaks observed for PVA, because during calcination at 400°C all the PVA molecules were decomposed.

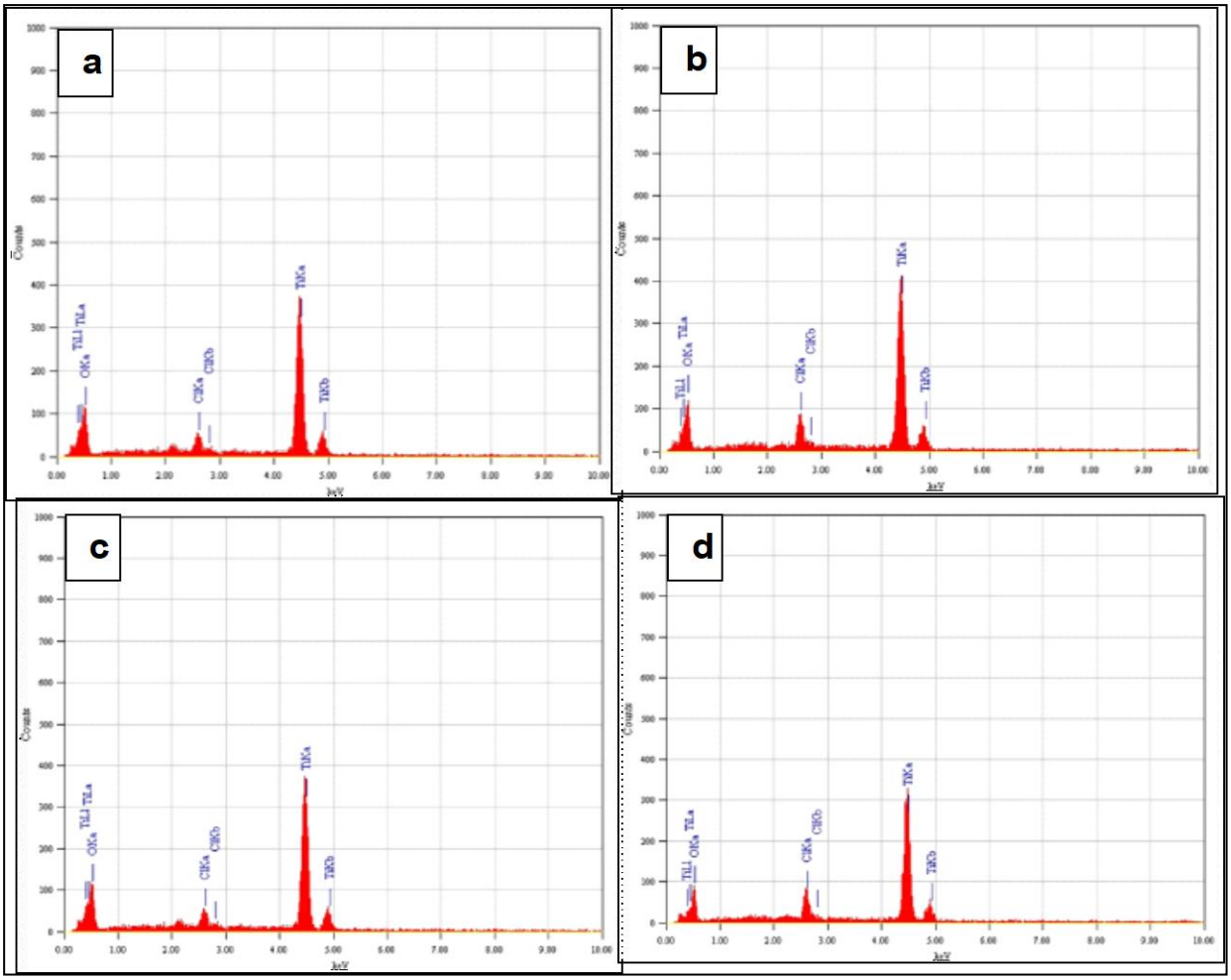

Fig. 4: EDAX analysis of a) TiO_2 b) 1% PVA c) 2% PVA and d) 3% PVA modified TiO_2 nanoparticles

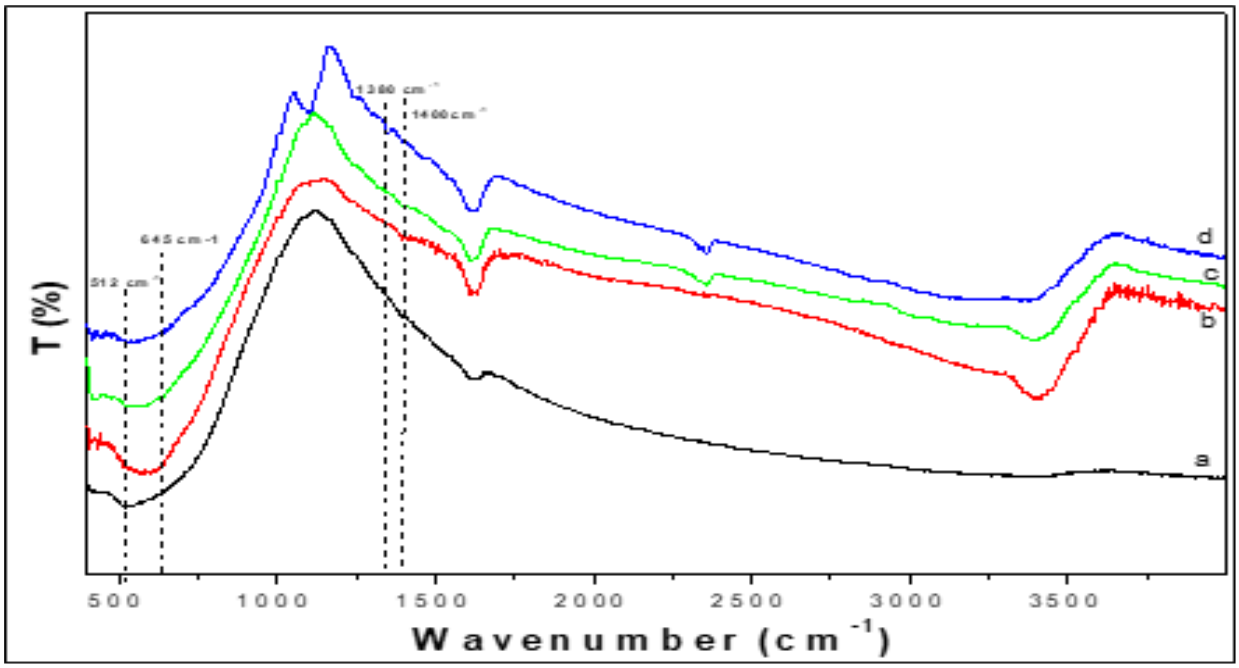

Fig. 5: FT-IR spectra of a) TiO_2 b) 1% PVA c) 2% PVA and d) 3% PVA modified TiO_2 nanoparticles.

3.5 Uv-Visible Spectroscopy

Fig. 6 shows the typical absorption spectrum of TiO_2 and PVA modified TiO_2 nanoparticles, respectively. In all the particles, the absorption was measured in the range between 250–700 nm. It is shown that TiO_2 is an oxide semiconductor and its anatase form has an optical absorbance range around 384 nm, bandgap 3.2 eV. In the current measurement, the onset of the absorption peak of maximum absorbance occurred at 372 nm for TiO_2. Further, it decreased with an increasing amount of PVA concentration. In PVA modified TiO_2 particles, the absorbance observed at 369, 360 and 350 nm for 1, 2 and 3% PVA, respectively. The blue shift in absorbance corresponds to a smaller particle size. The blue shift observed in the absorbance spectra indicated the Quantum confinement effect (Khanna *et al.* 2007). The absorption edge shifted to the lower wavelength region confirmed the formation of nano-sized product.

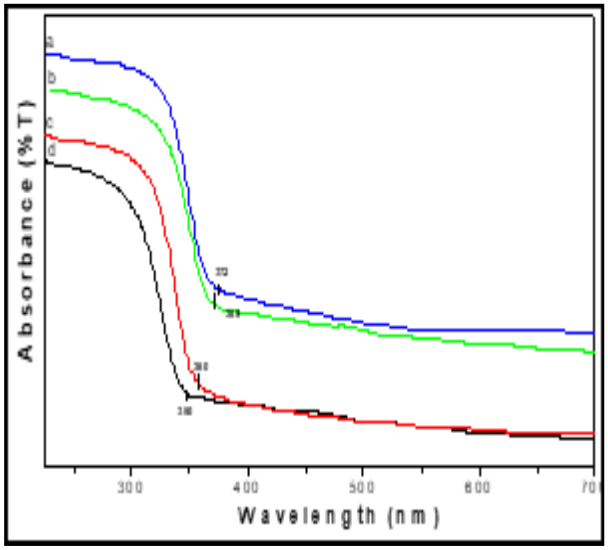

Fig. 6: Uv-Visible spectra of a) TiO_2 b) 1% PVA c) 2% PVA and d) 3% PVA modified TiO_2 nanoparticles

The measurement of the bandgap is important in semiconductors for photocatalytic and solar cell applications. The bandgap increased with increasing the amount of PVA concentration and it was showed in Fig.7. The optical bandgap of the material was calculated by effective mass approximation, and it was found to be 3.3, 3.36, 3.45 and 3.47 eV for TiO_2, 1, 2 and 3% PVA, respectively. These data strongly suggest that the bandgap increases with increasing concentrations of PVA. The optical bandgap of the material was calculated using effective mass approximation and was found to be higher than the bandgap of bulk TiO_2 (3.2 eV). However, the crystallite size of PVA modified TiO_2 particles prepared by the WCT was smaller than pure TiO_2, because of the quantum confinement effect (Dewi and Rini Mustiand, 2011).

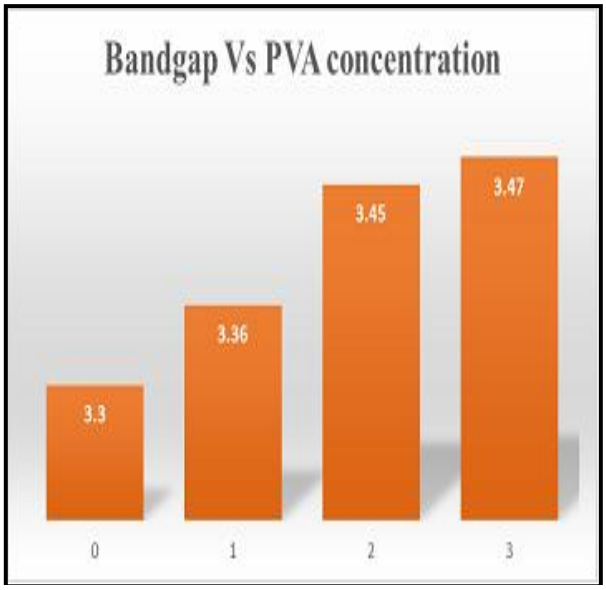

Fig. 7: Bandgap Vs PVA concentration.

3.6 Determination of Surface Area – B.E.T method

The BET specific surface areas of the samples calcined at 400ºC were 54 for TiO_2, and it gradually increases with increasing PVA concentration, and it was found to be 58, 61, and 63 for 1%, 2%, and 3% PVA modified TiO_2, respectively. The characterization of the PVA modified TiO_2 materials have been reported elsewhere. The surface area of the TiO_2 increased as a result of PVA concentration. It is possible that PVA form clusters within TiO_2 nanoparticle sphere thereby displacing some of the TiO_2 particles and increasing the surface area.

4. PHOTOCATALYTIC DECOMPOSITION OF ISOLAN BLUE

4.1 Effect of particle size on dye decomposition

Fig. 8 shows % decomposition vs time of isolan blue by TiO_2 various grain size (17 to 10 nm). The result shows that the TiO_2 grain size 10 nm shows the highest % decomposition. This is due to the fact that a reduction in the grain size increases the surface area and active sites on the photocatalyst, which in turn increases the adsorption of a number of isolan blue dye molecules. From the surface area measurements, it was found that increasing PVA concentration increases the surface area. So the high surface obtained at TiO_2 grain size10 nm shows the highest % of decomposition.

4.2 Effect of photocatalyst loading on decomposition

In order to avoid the use of excess catalyst, it is desirable to find out an optimum catalyst loading for

efficient decomposition. A series of experiments were carried out by varying the amount of catalyst from 10 to 30 mg/L with dye concentration of 50 mg/L, pH 8 and grain size 10 nm. The decomposition efficiency of isolan blue for various concentration of photocatalyst loading is illustrated in Fig.9. The results show that an increase in the catalyst loading from 10 to 25 mg/L increases the dye decomposition sharply from 68.75 to 96.25 %. This is due to the fact that an increase in catalyst loading increases the adsorption of a number of isolan blue species and hence the proportion of the excited species by incoming photons. Therefore the percentage of decomposition increases with higher catalyst loading. With an increase in the catalyst loading from 10 to 25 mg/L, the decomposition increases, suggesting that the optimum level for catalyst effectiveness has been attained for this amount of isolan blue 50 mg/L, further increase of the catalyst loading beyond 25mg/L resulted in a decrease in decomposition percentage of the dye. This phenomenon may be due to the hindrance and blocking of light penetration caused by the excessive amount of photocatalyst (Kim *et al.* 2006). On the other hand, at a higher concentration of the catalysts, particle aggregation is significantly reducing, thereby the active sites on the catalyst surface. Therefore the decomposition also reduced. So the optimum level of catalyst is 25 mg/L, with a dye concentration of 50 mg/L. Since the maximum decomposition of isolan blue is observed with 25 mg/L of TiO_2 photocatalyst and grain size 10 nm. The other experiments were carried out using 25 mg/L of TiO_2 nanoparticles.

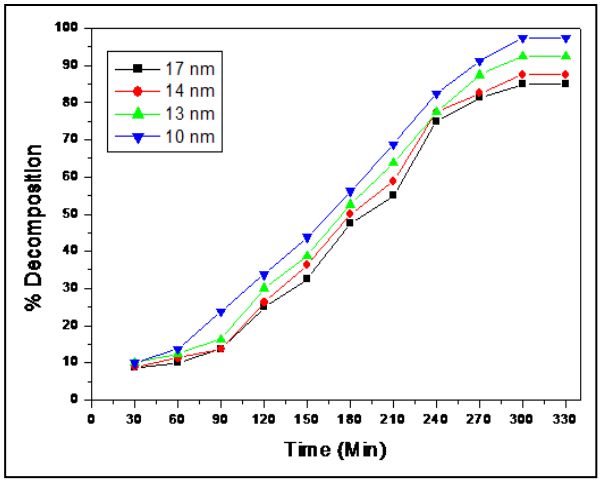

Fig. 8: Plot of % decomposition Vs Time at various particle size.

4.3 Effect of dye concentration

Fig. 10 shows the plot of % decomposition vs time with respect to different dye concentrations (10-70 mg/L). By varying the initial dye concentration from 10-70 mg/L of isolan blue solutions at a constant catalyst loading 25 mg/L, grain size 10nm at pH 8. It shows the highest decomposition only at a low concentration of the dye (10-50mg/L), which was due to the adsorption of dye molecules on to the nanoparticles and immediate degradation of the same. The results show that an increase in the dye concentration of more than 50 mg/L, decrease the decomposition of dye molecules.

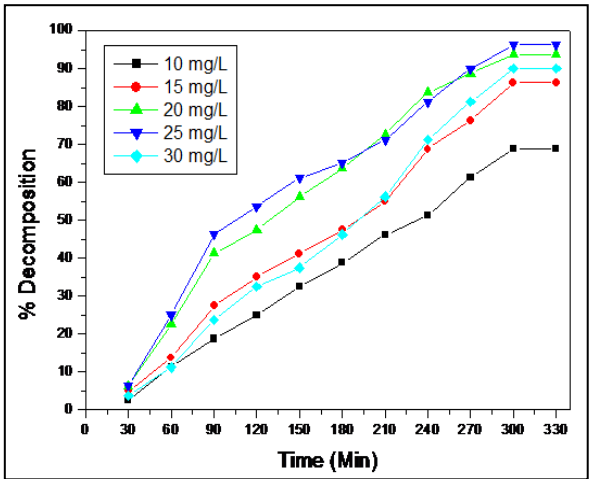

Fig. 9: Plot of % decomposition Vs Time at various photocatalyst concentration.

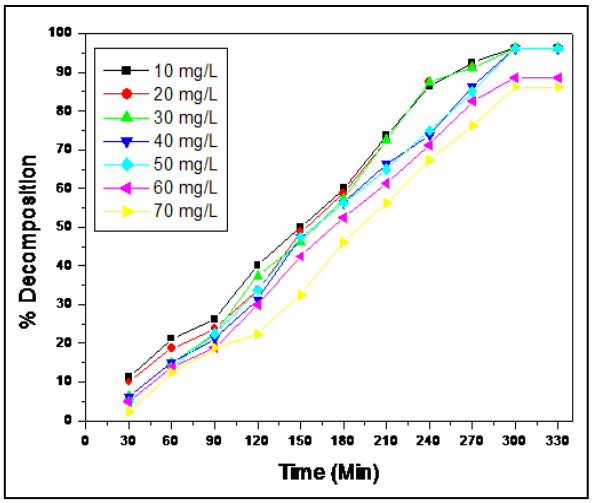

Fig. 10: Plot of % decomposition Vs Time at various dye concentration.

4.4 Effect of pH

The effect of pH on the decomposition of the dye by TiO_2 nanoparticles is shown in Fig. 11. The decomposition studies were carried out under both acidic and basic pH at constant dye concentration 50mg/L and constant TiO_2 concentration 25 mg/L. At an optimum concentration of dyes in both acidic and basic pH it seems to decrease the percentage decomposition of the dye. The increased effect seems to be more pronounced in the alkaline pH 8. The pH

affects not only the surface properties of TiO_2 but also the dissociation of dyes and the formation of hydroxyl radical. The importance of each one depends on the substrate nature and pH (Mengyeu *et al.* 1995). In acidic pH, TiO_2 gets agglomerated. So the surface area available for dye adsorption and photon adsorption would be reduced (Fox and Dulay, 1993). Under alkaline pH, OH^o ions are easier to be generated by oxidizing more hydroxide ions available on TiO_2 surface. Thus the efficiency of the process is increased (Concalves *et al.* 1991).

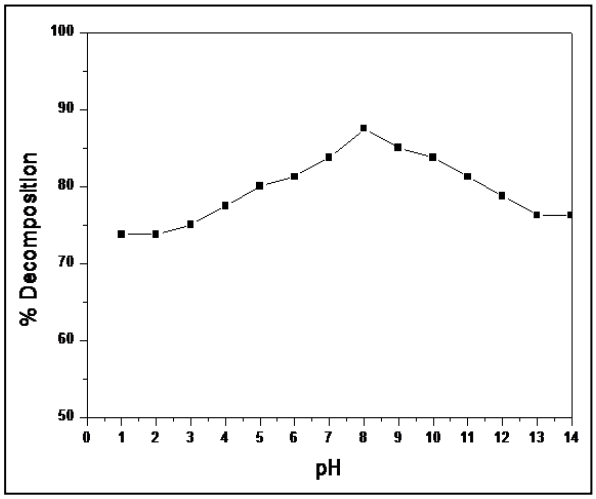

Fig. 11: Effect of pH on decomposition of dyes.

4.5 Mechanism of Photocatalysis

When light with energy equal to or higher than bandgap, it causes molecular excitation in the photocatalyst. As a result, it generates electron and holes in the conduction and valence band, respectively. After this process, the photocatalytic reactions will occur through a series of chemical reactions, for the formation of OH^o takes place. The reaction of OH^o with organic pollutants is the most important step that leads to the mineralization of organic pollutants to CO_2 and H_2O.

$$TiO_2 \rightarrow h^+ + e^-$$

$$OH^- + h^+ \rightarrow OH^o$$

$$O_2 + e^- \rightarrow O^o{}_2^-$$

$$O^o{}_2^- + H^+ \rightarrow HO^O{}_2$$

$$HO^O{}_2 + e^- \rightarrow HO_2^-$$

$$HO_2^- + H^+ \rightarrow H_2O_2$$

$$H_2O_2 + e^- \rightarrow OH^- + OH^o$$

$$IB + HO^o \rightarrow CO_2 + H_2O$$

4.6 Results of full-spectrum scan

Fig.12. shows the full spectrum scan of Isolan blue within 5 hr reaction at pH 8, dye concentration 50 mgL^{-1} and TiO_2 concentration 25 mgL^{-1} with particle size 10 nm. The primary adsorption peaks of the original dye solution are 375 nm and 575 nm in the spectral range of 300 to 750 nm. As the reaction time increases, the two peaks disappear gradually, and the full-spectrum scanning pattern changes obviously after 5 hr, at the end of the 5 hr reaction time, there is no evident adsorption peak observed at 375 and 575 nm. The adsorption also decreased. It indicates that the original chromophores in the dye solution are decomposed in the photocatalytic reaction and proves that isolan blue is decomposed in the solar/TiO_2 system.

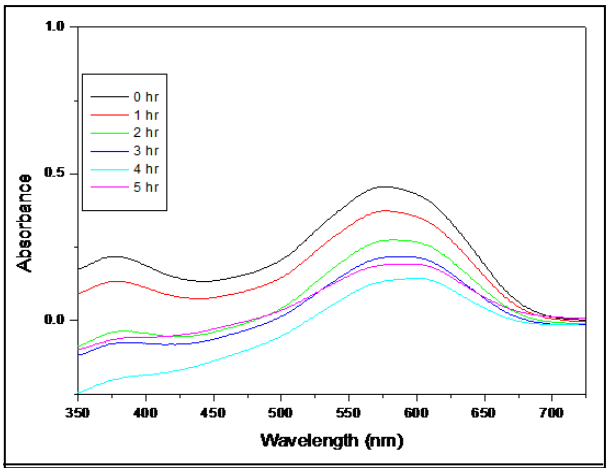

Fig. 12: Full spectrum scan of photocatalytic decomposition of Isolan blue by TiO_2 nanoparticles

4.7 Investigation on biodegradability

COD of the water sample before and after decomposition was estimated by 0.1N $K_2Cr_2O_7$ solution. The COD level decreased from the initial concentration 41.5 mg/L to 9.4 mg/L. The data indicate that the non-biodegradable organic part of the dye molecule was decomposed and mineralized in the photocatalytic process during the 5 hr reaction time. This indicates that there were fewer organic compounds that were difficult to biodegrade after the decomposition of Isolan Blue.

5. CONCLUSION

PVA modified TiO_2 nanoparticles were synthesized by a wet chemical technique. The decrease in grain size by increasing the PVA concentration was confirmed by XRD and TEM analysis. The blue shift in absorbance and increase in bandgap shows that the nanoparticles were suitable for photocatalytic applications. EDAX and FT-IR confirm the presence of the Ti and O bond. The nanoparticles show good photocatalytic activity, and they decompose the Isolan

Blue industrial dye within 5 hr reaction under solar radiation, and the nanoparticles were well suitable for environmental applications.

REFERENCES

Akpan, U. G. and Hameed, B. H., Parameters affecting the photocatalytic degradation of dyes using TiO_2-based photocatalysts: A review, *J. Hazard. Mater.*, 170(2-3), 520-529 (2009). https://dx.doi.org/10.1016/j.jhazmat.2009.05.039

Bao, J., Cai, Y., Sun, M., Wang, G. and Corke, H., Anthocyanins, flavonols and free radical scavenging activity of Chinese bayberry (*Myrica rubra*) extracts and their color properties a nd stability, *J. Agric. Food Chem.*, 53(6), 2327-2332 (2005). https://dx.doi.org/10.1021/jf048312z

Beydoun, D., Amal, R., Low, G. and McEvoy, S., Role of nanoparticles in photocatalysis, *J. Nanopart. Res.*, 1(1), 439–458 (1999). https://dx.doi.org/10.1023/A:1010044830871

Concalves, M. S. T., Oliveira-Campos, A. M. F., Pinto, E. M. M. S., Plasencia, P. M. S. and Queiroz, M. J. R. P. Q., Photochemical treatment of solutions of azo dyes containing TiO_2, *Chemosphere*, 39(5), 781-786 (1991). https://dx.doi.org/10.1016/S0045-6535(99)00013-2

Dewi, T., Rini, S., Musti, K. and Widuri, Modification of TiO_2 Nanoparticle with PEG and SiO_2 for anti-fogging and self-cleaning application**,** *Int. J. Engg. Technol.*, 11(73), 80-85 (2011).

Dong, J., Yao, X., Bo, H., Dong, W. and Yuhan, S., A Simple non-aqueous route to anatase TiO_2, *Eur. J. Inorg. Chem.*, 8, 1236–1240 (2008). https://dx.doi.org/10.1002/ejic.200700650

Fox, M. A. and Dulay, M. T., Heterogeneous photocatalysis, *Chem. Rev.*, 93(1), 341–357 (1993). https://dx.doi.org/10.1021/cr00017a016

Fox, M. A. and Dulay, M. T., Heterogeneous photocatalysis, *Chem. Rev.*, 93(1), 341-357 (1993). https://dx.doi.org/10.1021/cr00017a016

Fujishima, A., Rao, T. N. and Tryk, D. A., Titanium dioxide photocatalysis, *J. Photochem. Photobiol. C: Photochem. Rev.*, 1(1), 01-21 (2000). https://dx.doi.org/10.1016/S1389-5567(00)00002-2

Garbassi, F. and Balducci, L., Preparation and characterization of spherical TiO_2–SiO_2 particles, *Micropor. Mesopor. Mater.*, 47(1), 51-59 (2001). https://dx.doi.org/10.1016/S1387-1811(01)00302-X

Gomez, R., Lopez, T., Ortiz-Islas, E., Navarrete, J., Sanchez, E., Tzompanztzi, F. and Bokhimi, X., Effect of sulfation on the photoactivity of TiO_2 sol–gel derived catalysts, *J. Mol. Catal. A: Chem.*, 193(1-2), 217–226 (2003). https://dx.doi.org/10.1016/S1381-1169(02)00473-9

Herrmann, J. M., Heterogeneous photocatalysis: Fundamentals and applications to the removal of various types of aqueous pollutants, *Catal. Today.*, 53(1), 115-129 (1999). https://dx.doi.org/10.1016/S0920-5861(99)00107-8

Hoffmann, M. R., Martin, S. T., Choi, W. and Bahnemann, D. W., Elemental applications of semiconductor photocatalysis, *Chem. Rev.*, 95(1), 69-96 (1995). https://dx.doi.org/10.1021/cr00033a004

Hsuan-Fu, Y. and W. Shenq-Min, Effects of water content and pH on gel-derived TiO_2-SiO_2, *J. Non-Cryst. Sol.*, 261(1-3), 260-267 (2000). https://dx.doi.org/10.1016/S0022-3093(99)00658-4

Hua, L., Guang, Y., Aiping, C., Yuhua, L. and Peixiang, L., Growth and characteristics of laser deposited anatase and rutile TiO_2 films on Si substrates, *Thin Solid Films*, 517, 745–749 (2008). https://dx.doi.org/10.1016/j.tsf.2008.08.179

Hussain, M., Ceccarelli, R., Marchisio, D. L., Fino, D., Russo, N. and Geobaldo, F., Synthesis, characterization, and photocatalytic application of novel TiO_2 nanoparticles, *Chem. Eng. J.*, 157(1), 45–51 (2010). https://dx.doi.org/10.1016/j.cej.2009.10.043

Khanna, P. K., Singh, N. and Shobhit, C., Synthesis of nano-particles of anatase-TiO_2 and preparation of its optically transparent film in PVA, *Mat. Lett.*, 61(25), 4725 - 4730 (2007). https://dx.doi.org/10.1016/j.matlet.2007.03.064

Kim, D. S., Park, Y. S., Photocatalytic decolorization of Rhodamine B by immobilized TiO_2 onto silicone sealant, *Chem. Eng. J.*, 116(2), 133–137 (2006). https://dx.doi.org/10.1016/j.cej.2005.10.013

Konstantinou, I. K. and Albanis, T. A., TiO_2-Assisted photocatalytic degradation of azo dyes in aqueous solution: Kinetic and mechanistic investigations—A review, *Appl. Catal. B: Environ.*, 49(1), 01–14 (2004). https://dx.doi.org/10.1016/j.apcatb.2003.11.010

Kumar, K. N. P., Jalajakumari, K. and Keizer, K., Effect of peptization on densification and phase-transformation behavior of sol-gel-derived nanostructured Titania, *J. Am. Ceram. Soc.*, 77(5), 1396-1400 (1994). https://dx.doi.org/10.1111/j.1151-2916.1994.tb05426.x

Mahadwad, O. K., Parikh, P. A., Jasra, R. V. and Patil, C., Photocatalytic degradation of reactive black-5 dye using TiO_2 impregnated ZSM-5, *Bull. Mater. Sci.*, 34(3), 551–556 (2011). https://dx.doi.org/10.1007/s12034-011-0124-2

Malladi, S., Mallikarjunagouda, B. P., Ravindra, S. V., Sangamesh, A. P. and Tejraj, M. A., Novel dense poly (vinyl alcohol)–TiO_2 mixed matrix membranes for pervaporation separation of water–isopropanol mixtures at 30 °C**,** *J. Mem. Sci.*, 281(1-2), 95-102 (2006). https://dx.doi.org/10.1016/j.memsci.2006.03.022

Mengyue, Z., Shifu, C. and Yaowu, T., Photocatalytic degradation of organophosphorus pesticides using thin films of TiO_2, *J. Chem. Tech. Biotechnol.*, 64, 339–344 (1995). https://dx.doi.org/10.1002/jctb.280640405

Music, S., Gotic, M., Ivanda, M., Popovic, S., Turkovic, A., Trojko, R., Sekulic, A. and Furic, K., Chemical and micro structural properties of TiO_2 synthesized by sol-gel procedure, *Mater. Sci. Eng. B*, 47(1), 33-40 (1997). https://dx.doi.org/10.1016/S0921-5107(96)02041-7

Nguyen, V-C. and Nguyen, T-V., Photocatalytic removal of phenol under natural sunlight over N-TiO_2-SiO_2 catalyst: The effect of nitrogen composition in TiO_2-SiO_2, *Environment Asia*, 2(1), 23-29 (2009). https://dx.doi.org/10.14456/ea.2009.4

Selvaraj, A., Parimiladevi, R., Rajesh K.B., Synthesis of nitrogen doped titanium dioxide (TiO_2) and its photocatalytic performance for the degradation of Indigo Carmine Dye, *J. Environ. Nanotechnol.,* 2(1), 35-41 (2013). https://dx.doi.org/10.13074/jent.2013.02.121026

Shankar, V., Gessesse, M., Obare, S. O. and Ramakrishna, G., Dynamics and two-photon absorption properties of chromophore functionalized semiconductor nanoparticles, *Proc. of SPIE* 7413, 741309-741401 (2009). https://dx.doi.org/10.1117/12.829276

Sushil Kumar Kansal, Swati Sood, Ahmad Umar and Mehta, S. K., Photocatalytic degradation of Eriochrome Black T dye using well-crystalline anatase TiO_2 nanoparticles, *J. Alloys Compd*., 581, 392–397 (2013). https://dx.doi.org/10.1016/j.jallcom.2013.07.069

Tang, W. Z. and An, H., UV/TiO_2 Photocatalytic oxidation of commercial dyes in aqueous solutions, *Chemosphere*, 31(9), 4157–4170 (1995). https://dx.doi.org/10.1016/0045-6535(95)80015-D

Vilma, C. C., Lameiras, F. Sansviero, T. M. C., Simoes, A. B. and Vasconcelos, W. L., Preparation of CdS-containing silica–titania composites by the sol–gel process, *J. Non-Cryst. Solids.*, 348, 190–194 (2004). https://dx.doi.org/10.1016/j.jnoncrysol.2004.08.167

Wang, D., Song, C., Lin, Y. and Hu, Z., Preparation and characterization of TiO_2 hollow spheres, *Mater. Lett*., 60(1), 77-80 (2006). https://dx.doi.org/10.1016/j.matlet.2005.07.076

Yusuf, M. M., Imai, H. and Hirashima, H., Preparation of porous titania film by modified sol-gel method and its application to photocatalyst, *J. Sol-Gel Sci. Tech.*, 25, 65-74 (2002). https://dx.doi.org/10.1023/A:1016045111857

Zhang, X. and Zheng, H., Synthesis of TiO_2-doped SiO_2 composite films and its applications, *Bull. Mater. Sci.*, 31(5), 787–790 (2008). https://dx.doi.org/10.1007/s12034-008-0125-y